

Period-luminosity relations of type II Cepheids in the Magellanic Clouds

Noriyuki Matsunaga^{1*}, Michael W. Feast^{2,3} and Igor Soszyński⁴

¹ Kiso Observatory, Institute of Astronomy, School of Science, the University of Tokyo, 10762-30, Mitake, Kiso, Kiso, Nagano 397-0101, Japan

² South African Astronomical Observatory, PO Box 9, Observatory, 7935, South Africa

³ Astrophysics, Cosmology and Gravitation Centre and Department of Astronomy, University of Cape Town, Rondebosch, 7701, South Africa

⁴ Warsaw University Observatory, Al. Ujazdowskie 4, 00-478 Warszawa, Poland

Accepted 2010 November 29. Received 2010 November 24; in original form 2010 July 22

ABSTRACT

Period-luminosity relations (PLRs) of type II Cepheids (T2Cs) in the Small Magellanic Cloud are derived based on OGLE-III, IRSF/SIRIUS and other data, and these are compared with results for the Large Magellanic Cloud and Galactic globular clusters. Evidence is found for a change of the PLR slopes from system to system. Treating the longer period T2Cs (W Vir stars) separately gives an SMC-LMC modulus difference of 0.39 ± 0.05 mag without any metallicity corrections being applied. This agrees well with the difference in moduli based on different distance indicators, in particular the PLRs of classical Cepheids. The shorter period T2Cs (BL Her stars) give a smaller SMC-LMC difference suggesting that their absolute magnitudes might be affected either by metallicity or by age effects. It is shown that the frequency distribution of T2C periods also changes from system to system.

Key words: Cepheids – stars: distances – Magellanic Clouds – infrared: stars.

1 INTRODUCTION

Cepheids are pulsating stars with periods between one day and about one hundred days. Although there was originally some confusion, see the review by Fernie (1969), it is now believed that Cepheids can be grouped into two distinct classes: classical Cepheids and type II Cepheids (T2Cs, hereafter). The former are intermediate mass stars ($4\text{--}10 M_{\odot}$), while the latter are lower-mass stars ($\sim 1 M_{\odot}$) belonging to disc and halo populations (Wallerstein 2002; Sandage & Tammann 2006).

T2Cs are conventionally divided into three period groups, BL Her stars (henceforth BL) at short periods, W Vir stars (WV) at intermediate periods and RV Tau stars (RV) at the longest periods. According to Gingold (1976, 1985), the BLs are stars evolving from the horizontal branch to the Asymptotic Giant Branch (AGB); the WVs are stars that along the AGB cross the Cepheid instability strip due to excursions towards higher effective temperatures; the RVs are stars that after their AGB phase are moving towards the white dwarf cooling sequence. However, some later evolutionary tracks (e.g. Pietrinferni et al. 2006) do not show the excursions, and the precise evolution state of T2Cs remains unclear. We follow the division by Soszyński et al. (2008b) and adopt thresholds of 4 d and 20 d to divide the three groups. The RV stars tend to show alternating deep and shallow minima (and this is often taken as a defining characteristic), but the single period of the RVs will be used in this paper. In addition to these three groups, Soszyński et al. (2008b)

established a new group of T2Cs, peculiar W Vir (pW) stars. They have distinctive light curves and tend to be brighter than normal T2Cs of the same period. It is suggested that many, perhaps all, of them are binaries, but their nature remains uncertain. The bright Galactic T2C κ Pav appears to be a pW star (Matsunaga, Feast & Menzies, 2009, hereafter M09).

Matsunaga et al. (2006, hereafter M06) discovered a tight PLR of T2Cs in globular clusters based on infrared photometry for 46 T2Cs. Feast et al. (2008) used pulsation parallaxes of nearby T2Cs to calibrate this cluster PLR and to discuss the distances of the Large Magellanic Cloud (LMC) and the Galactic Centre. The Optical Gravitational Lensing Experiment (OGLE-III) have significantly increased samples of T2Cs in the Magellanic Clouds. Soszyński et al. (2008b) found 197 T2Cs in the LMC. M09 investigated their near-infrared (near-IR) nature and confirmed that BL and WV stars follow a tight PLR like that of T2Cs in globular clusters, whereas RV and pW stars show a large scatter and are systematically brighter than the PLR for the BL and WVs. The calibration by Feast et al. (2008) then leads to a distance modulus of the LMC of 18.46 ± 0.05 mag. These investigations have established the T2Cs as a promising distance indicator.

The aim of the present paper is to compare the T2C PLRs in the Small Magellanic Cloud (SMC), LMC and globular clusters. This is important for a further study of these relations and their possible dependence on metallicity and other factors. The OGLE-III survey discovered 43 T2Cs in the SMC (Soszyński et al. 2010b, S10 hereafter). In the following, we first collect near-IR *JHK* magnitudes of SMC T2Cs (Section 2) and investigate their PLRs

* E-mail: matsunaga@ioa.s.u-tokyo.ac.jp

(Section 3). The reddening-free PLR in VI is also discussed. In parallel with our work, Ciechanowska et al. (2010, C10) have obtained independent J and K for a subset of the SMC T2Cs and their data is combined with ours in some of the discussions. We find evidence that the BL and WV stars need to be discussed independently. In Section 4 the apparent differences in distance moduli of the LMC and SMC are derived for these stars and compared with the differences obtained from other objects. The data used for classical Cepheids are discussed in an Appendix. In addition, the colours and period distributions of T2Cs in various systems are compared and contrasted in Sections 5. Section 6 summarizes the present work.

2 INFRARED PHOTOMETRY

S10 catalogued 43 T2Cs in the SMC: 17 BLs, 10 WVs, 7 pWVs and 9 RVs. We searched for near-IR counterparts of these stars in the catalogue of Kato et al. (2007). This point-source catalogue is based on simultaneous images in JHK_s obtained with the 1.4-m Infrared Survey Facility (IRSF) located at South African Astronomical Observatory (SAAO), Sutherland, South Africa. The catalogue covers 40 deg^2 of the LMC, 11 deg^2 of the SMC and 4 deg^2 of the Magellanic Bridge. The catalogue extends to fainter magnitudes and has higher resolution than the point-source catalogue of the Two-Micron All-Sky Survey (2MASS; Skrutskie et al. 2006) in the regions of the Magellanic Clouds. The 10σ limiting magnitudes of the survey in the SMC are 18.9, 17.9 and 16.9 mag for J , H and K_s . These limits are fainter than those for the LMC since the crowding effect is less (Kato et al. 2007).

Matches between the OGLE-III and IRSF catalogues were found for 39 S10 T2C sources with a tolerance of $0.5''$ (Table 1). The differences in coordinates are small between the catalogues with standard deviations of less than $0.1''$ in both RA and Dec. Four OGLE-III sources (IDs in S10: #5, #37, #42 and #43) are located outside the IRSF survey field. In the case of two matched objects, #6 and #22, K_s -band magnitudes are missing because of the faintness of these stars, both of which are BL stars with relatively short periods ($P < 1.5 \text{ d}$). Although about half of the BL sample have K_s fainter than the 10σ limiting magnitude, their J and H magnitudes are brighter than the limits.

We have compared our photometry with that obtained by C10, who used the SOFI infrared camera attached to the ESO New Technology Telescope (NTT) to obtain photometry in J and K for 19 OGLE-III T2Cs in the SMC (14 BLs and 5 WVs). C10 observed three of them twice and the others once. Excluding three objects not included in the IRSF survey, there are 19 measurements for the T2Cs common with ours. Their magnitudes are listed by C10 in the 2MASS system. They were transformed into the IRSF/SIRIUS system (Kato et al. 2007) before compared with our photometry. Additionally, the OGLE-III (S10) periods and epochs of maximum I were used to calculate the phases for both the NTT observations and the IRSF ones and to estimate the difference ΔI between the two phases. Fig. 1 plots the difference between their photometry and ours against the variation predicted from the I -band light curves. The plots show a reasonable correlation which indicates that the NTT photometry is in agreement with our IRSF photometry. It also supports the assumption that the I -band light curves reasonably predict the near-infrared variations as suggested in M09, so

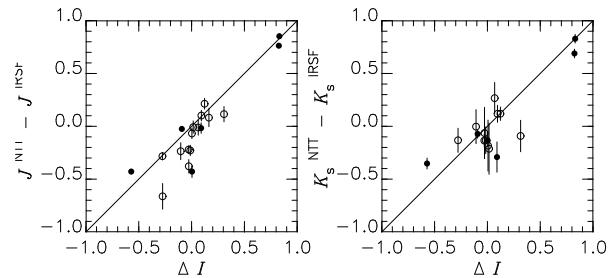


Figure 1. Differences between the IRSF photometry and the NTT photometry (C10) are plotted against the predicted differences from the I -band light curves. BL stars are indicated by open circles and WV stars by filled circles.

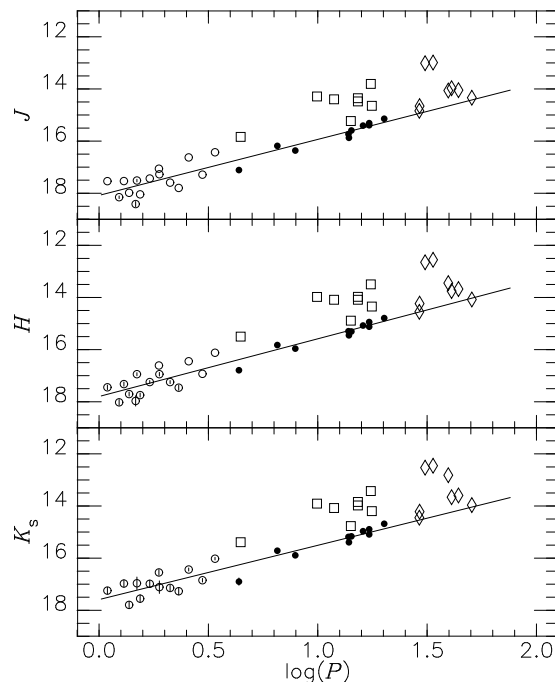


Figure 2. Period-magnitude relations of T2Cs in the SMC. The phase-corrected JHK_s magnitudes are plotted against periods. Open circles indicates BL stars and filled circles WV stars. The lines show the PLRs for the combined sample of BLs and WVs. RV and pW stars are indicated by diamond symbols and squares. Error bars are drawn if the photometric errors are larger than 0.05 mag.

that we adopt the phase correction used by M09 to estimate mean magnitudes¹.

3 PERIOD-LUMINOSITY RELATIONS OF TYPE II CEPHEIDS

3.1 PLRs of the SMC T2Cs

Fig. 2 shows the phase-corrected JHK_s data plotted against $\log P$ for the SMC T2Cs based on our data alone. The BL and WV stars

¹ Phase-corrected data are used throughout this paper although C10 found that this did not reduce the scatter for their sample of stars. None of the conclusions of the paper are significantly affected if uncorrected data are used.

Table 1. The catalogue of OGLE-III T2Cs in the SMC with IRSF counterparts. Modified Julian Dates (MJD), pulsation phase of the observations, JHK_s magnitudes and their errors are listed for each IRSF measurement as well as the OGLE-IDs, types and periods. Shifts for the phase corrections (δ_ϕ) obtained from the I -band light curves are also listed. Two sources, #28 and #35, are listed twice because they are located in overlapping fields of the IRSF survey.

OGLE-ID	Type	log P	IRSF counterpart									δ_ϕ
			IRSF-Field	MJD(obs)	Phase	J	E_J	H	E_H	K_s	E_{K_s}	
1	pWVir	1.07441	SMC0031-7350F	52847.100	0.944	14.32	0.01	14.01	0.01	14.00	0.01	0.076
2	BLHer	0.13741	SMC0037-7250C	52518.027	0.115	17.84	0.04	17.56	0.08	17.65	0.14	0.145
3	WVir	0.63947	SMC0036-7350G	52849.096	0.677	17.27	0.03	16.95	0.04	17.06	0.14	-0.160
4	WVir	0.81514	SMC0037-7310A	52517.858	0.911	16.16	0.04	15.80	0.04	15.69	0.05	0.025
6	BLHer	0.09188	SMC0041-7330A	52494.999	0.263	18.06	0.05	17.93	0.11	-	-	0.094
7	RVTau	1.49081	SMC0041-7310D	52496.056	0.372	13.10	0.01	12.74	0.01	12.62	0.02	-0.090
8	BLHer	0.17312	SMC0046-7330I	53413.759	0.552	17.60	0.05	17.03	0.06	17.05	0.24	-0.086
9	BLHer	0.47291	SMC0046-7250C	52457.193	0.867	17.17	0.03	16.81	0.03	16.73	0.07	0.118
10	pWVir	1.24256	SMC0046-7330E	53301.789	0.454	13.83	0.02	13.52	0.02	13.45	0.02	-0.025
11	pWVir	0.99675	SMC0046-7330E	53301.789	0.451	14.34	0.01	14.03	0.01	13.96	0.02	-0.052
12	RVTau	1.46566	SMC0046-7310B	53397.808	0.477	14.70	0.01	14.28	0.01	14.26	0.02	-0.044
13	WVir	1.14019	SMC0046-7250B	52457.177	0.216	15.73	0.01	15.29	0.02	15.18	0.02	0.004
14	WVir	1.14234	SMC0050-7330I	52517.837	0.622	15.98	0.02	15.56	0.02	15.50	0.03	-0.107
15	BLHer	0.40986	SMC0050-7310E	52517.914	0.223	16.59	0.02	16.41	0.03	16.40	0.06	0.037
16	BLHer	0.32494	SMC0050-7250H	52518.878	0.222	17.51	0.03	17.16	0.06	17.06	0.12	0.084
17	BLHer	0.11371	SMC0051-7130B	52534.061	0.483	17.60	0.04	17.39	0.08	17.04	0.14	-0.067
18	RVTau	1.59681	SMC0050-7350G	52894.012	0.409	14.36	0.02	13.75	0.01	13.12	0.01	-0.301
19	RVTau	1.61185	SMC0055-7330C	52868.173	0.867	13.93	0.02	13.71	0.01	13.62	0.02	0.043
20	RVTau	1.70435	SMC0055-7230C	52518.940	0.088	14.11	0.02	13.85	0.02	13.74	0.02	0.226
21	BLHer	0.36420	SMC0055-7250F	52842.164	0.890	17.77	0.04	17.43	0.10	17.24	0.14	0.029
22	BLHer	0.16747	SMC0055-7350E	52950.854	0.627	18.64	0.10	18.19	0.20	-	-	-0.222
23	pWVir	1.24737	SMC0055-7310E	52837.125	0.356	14.68	0.01	14.38	0.01	14.23	0.02	-0.034
24	RVTau	1.64307	SMC0055-7330H	52835.157	0.504	14.11	0.01	13.74	0.01	13.66	0.02	-0.065
25	pWVir	1.15140	SMC0055-7310D	52837.106	0.342	15.28	0.02	14.94	0.01	14.82	0.02	-0.050
26	BLHer	0.23168	SMC0059-7210F	53300.954	0.988	17.38	0.03	17.19	0.06	16.93	0.14	0.055
27	BLHer	0.18801	SMC0100-7330F	52844.081	0.752	18.11	0.04	17.81	0.08	17.62	0.15	-0.067
28	pWVir	1.18368	SMC0055-7330D	52835.090	0.595	14.58	0.01	14.19	0.01	14.08	0.02	-0.102
28	pWVir	1.18368	SMC0100-7330F	52844.081	0.184	14.32	0.01	13.94	0.01	13.81	0.01	0.034
29	RVTau	1.52733	SMC0059-7210C	52530.910	0.330	13.07	0.01	12.64	0.01	12.54	0.01	-0.084
30	BLHer	0.53006	SMC0100-7310I	52847.141	0.310	16.43	0.01	16.12	0.03	16.02	0.05	-0.000
31	WVir	0.89737	SMC0059-7130H	52530.855	0.241	16.36	0.02	15.96	0.03	15.89	0.05	0.003
32	WVir	1.15372	SMC0100-7330B	52844.177	0.161	15.50	0.02	15.21	0.01	15.07	0.02	0.093
33	BLHer	0.27362	SMC0059-7230E	53300.908	0.738	17.29	0.02	16.84	0.04	16.78	0.11	-0.232
34	WVir	1.30364	SMC0059-7210B	52530.895	0.047	14.84	0.02	14.49	0.01	14.38	0.02	0.302
35	WVir	1.23506	SMC0100-7350D	53355.802	0.706	15.46	0.02	15.19	0.02	15.16	0.04	-0.069
35	WVir	1.23506	SMC0100-7350E	52956.766	0.481	15.86	0.02	15.49	0.02	15.44	0.05	-0.548
36	BLHer	0.03809	SMC0104-7310F	52869.164	0.853	17.52	0.04	17.43	0.09	17.23	0.13	0.017
38	pWVir	0.64778	SMC0104-7330B	52849.160	0.297	15.82	0.02	15.48	0.02	15.37	0.03	0.020
39	BLHer	0.27590	SMC0109-7310F	52956.779	0.398	17.31	0.03	16.98	0.07	17.15	0.24	-0.037
40	WVir	1.20712	SMC0108-7150D	53315.777	0.985	15.04	0.01	14.71	0.01	14.60	0.04	0.367
41	RVTau	1.46417	SMC0113-7310B	52960.863	0.944	14.78	0.01	14.49	0.01	14.39	0.02	0.060

(the filled circles) show well defined PLRs in all the JHK_s bands. In contrast, pWs (squares) and RVs (open circles) show a large scatter and are brighter than the PLRs of the BL and WV stars. These objects are discussed in Section 5.

PLRs were calculated for BLs and WVs alone and for the combined sample of BL and WV stars. We also derived reddening-free PLRs for the S10 VI data using the indices, $W_i(VI) = I - R_i^{VI}(V - I)$, where $R_1^{VI} = 1.55$ and $R_2^{VI} = 1.45$ corresponding to two reddening laws as in M09. Table 2 also gives similar relations for the T2Cs in the LMC and those in globular clusters, using the data in M09 and M06. There is not sufficient data to derive PLRs in VI for the globular cluster objects.

Dispersions (σ) about the various PLRs are listed in Table 2. For the LMC/SMC samples, these tend to be greater for the BLs than for the WVs. Such differences though suggestive are of

only marginal significance. An extreme example is for the log $P - W_1(VI)$ in the SMC where σ is 0.26 for the BLs and 0.10 mag for the WVs. However, an F-test shows that this is not significant at the 95 % confidence level. In the case of the BL stars in the SMC the C10 data alone shows a smaller scatter (0.26 mag) than the IRSF data (0.37 mag) in K_s , which probably indicates a larger observational scatter for the faintest stars in the latter sample. It should be noted that in the case of the LMC we followed Soszyński et al. (2008b) and M09 in omitting a few bright BL stars as possible binaries or blends, while no BL stars were omitted from the SMC sample. Although no evidence of such binarity or blend has been reported for the SMC BL stars, this may well affect the comparison of the σ values.

Table 2. Period-luminosity relations of type II Cepheids. The slope, zero-point near the median period, residual scatter σ and the sample size N are listed for each group. The relations in JHK_s bands are derived using only the IRSF data. Those indicated as J^\dagger and K_s^\dagger are obtained from the combined IRSF and NTT (C10) datasets. The reddening-free indices $W_i(VI)$ are defined in the text. For the LMC/SMC JHK_s observations, phase corrections have been applied. Mean magnitudes were obtained from repeated photometry for globular clusters objects. The PLRs for globular clusters are from Matsunaga et al. (2006) and those for the LMC from Matsunaga et al. (2009).

Band	Group	Type	Slope	Zero (@ $\log P_0$)	σ	N
J	SMC	BL	-2.545 ± 0.764	17.393 ± 0.112 (@ 0.3)	0.41	15
J	SMC	WV	-2.667 ± 0.246	15.483 ± 0.059 (@ 1.2)	0.16	10
J	SMC	BL+WV	-2.147 ± 0.154	15.506 ± 0.116 (@ 1.2)	0.34	25
H	SMC	BL	-2.765 ± 0.731	17.080 ± 0.108 (@ 0.3)	0.40	15
H	SMC	WV	-2.655 ± 0.236	15.129 ± 0.057 (@ 1.2)	0.15	10
H	SMC	BL+WV	-2.214 ± 0.148	15.141 ± 0.112 (@ 1.2)	0.32	25
K_s	SMC	BL	-2.096 ± 0.732	16.933 ± 0.104 (@ 0.3)	0.37	13
K_s	SMC	WV	-2.844 ± 0.305	15.038 ± 0.073 (@ 1.2)	0.20	10
K_s	SMC	BL+WV	-2.082 ± 0.151	15.091 ± 0.109 (@ 1.2)	0.32	23
J^\dagger	SMC	BL	-2.690 ± 0.488	17.325 ± 0.069 (@ 0.3)	0.36	31
J^\dagger	SMC	WV	-2.460 ± 0.277	15.486 ± 0.073 (@ 1.2)	0.24	16
J^\dagger	SMC	BL+WV	-2.092 ± 0.116	15.495 ± 0.092 (@ 1.2)	0.33	47
K_s^\dagger	SMC	BL	-2.553 ± 0.444	16.924 ± 0.061 (@ 0.3)	0.32	29
K_s^\dagger	SMC	WV	-2.568 ± 0.247	15.041 ± 0.065 (@ 1.2)	0.22	16
K_s^\dagger	SMC	BL+WV	-2.113 ± 0.105	15.063 ± 0.082 (@ 1.2)	0.29	45
$W_1(VI)$	SMC	BL	-2.421 ± 0.479	16.832 ± 0.069 (@ 0.3)	0.26	17
$W_1(VI)$	SMC	WV	-3.003 ± 0.158	14.721 ± 0.040 (@ 1.2)	0.10	10
$W_1(VI)$	SMC	BL+WV	-2.304 ± 0.107	14.789 ± 0.083 (@ 1.2)	0.23	27
$W_2(VI)$	SMC	BL	-2.430 ± 0.488	16.894 ± 0.070 (@ 1.2)	0.27	17
$W_2(VI)$	SMC	WV	-2.985 ± 0.153	14.811 ± 0.039 (@ 0.3)	0.10	10
$W_2(VI)$	SMC	BL+WV	-2.277 ± 0.108	14.878 ± 0.085 (@ 1.2)	0.24	27
<hr/>						
J	LMC	BL	-2.164 ± 0.240	17.131 ± 0.038 (@ 0.3)	0.25	55
J	LMC	WV	-2.337 ± 0.114	15.165 ± 0.030 (@ 1.2)	0.18	82
J	LMC	BL+WV	-2.163 ± 0.044	15.194 ± 0.029 (@ 1.2)	0.21	137
H	LMC	BL	-2.259 ± 0.248	16.857 ± 0.039 (@ 0.3)	0.26	54
H	LMC	WV	-2.406 ± 0.100	14.756 ± 0.027 (@ 1.2)	0.16	82
H	LMC	BL+WV	-2.316 ± 0.043	14.772 ± 0.028 (@ 1.2)	0.20	136
K_s	LMC	BL	-1.992 ± 0.278	16.733 ± 0.040 (@ 0.3)	0.26	47
K_s	LMC	WV	-2.503 ± 0.109	14.638 ± 0.029 (@ 1.2)	0.17	82
K_s	LMC	BL+WV	-2.278 ± 0.047	14.679 ± 0.029 (@ 1.2)	0.21	129
$W_1(VI)$	LMC	BL	-2.598 ± 0.094	16.597 ± 0.017 (@ 0.3)	0.10	55
$W_1(VI)$	LMC	WV	-2.564 ± 0.073	14.333 ± 0.019 (@ 1.2)	0.11	76
$W_1(VI)$	LMC	BL+WV	-2.521 ± 0.022	14.339 ± 0.015 (@ 1.2)	0.11	131
$W_2(VI)$	LMC	BL	-2.572 ± 0.093	16.665 ± 0.016 (@ 0.3)	0.10	55
$W_2(VI)$	LMC	WV	-2.551 ± 0.073	14.431 ± 0.019 (@ 1.2)	0.11	76
$W_2(VI)$	LMC	BL+WV	-2.486 ± 0.022	14.440 ± 0.015 (@ 1.2)	0.11	131
<hr/>						
J	Globular	BL	-2.959 ± 0.313	-1.541 ± 0.041 (@ 0.3)	0.11	7
J	Globular	WV	-2.204 ± 0.090	-3.543 ± 0.027 (@ 1.2)	0.16	39
J	Globular	BL+WV	-2.230 ± 0.053	-3.542 ± 0.024 (@ 1.2)	0.16	46
H	Globular	BL	-2.335 ± 0.335	-1.847 ± 0.044 (@ 0.3)	0.12	7
H	Globular	WV	-2.337 ± 0.086	-3.942 ± 0.025 (@ 1.2)	0.16	39
H	Globular	BL+WV	-2.344 ± 0.050	-3.944 ± 0.023 (@ 1.2)	0.15	46
K_s	Globular	BL	-2.294 ± 0.294	-1.864 ± 0.039 (@ 0.3)	0.10	7
K_s	Globular	WV	-2.442 ± 0.082	-3.997 ± 0.024 (@ 1.2)	0.15	39
K_s	Globular	BL+WV	-2.408 ± 0.047	-4.004 ± 0.021 (@ 1.2)	0.14	46

3.2 Comments on the PLR slopes

Fig. 3 shows PLRs in J and K_s for the SMC based on the combined sample of C10 and the present paper. This consists of 16 measurements of BLs and 31 of WVs (29 at K_s), all of which were corrected for phase variation, for BLs and WVs. C10 derived a distance modulus of 18.85 mag for the SMC by comparing their combined BL+WV sample with the PLRs in J and K_s derived for globular cluster T2Cs by M06. In Fig. 3 these relations are shown as dashed lines for the distance derived by C10. The solid lines are

least square fits to the data. Apparently the dashed lines with the cluster slopes do not fit the data. This is particularly noticeable in K_s where the best fit with a line of cluster slope is too bright by 0.21 mag at $\log P = 1.3$ and too faint by 0.09 mag at $\log P = 0.3$. This discrepancy, although present, is not as clear from C10 data alone since they had only two long period WV stars.

The slopes listed in Table 2 show that, in fact, there is a general trend for the PLR slopes to become more negative as one goes from the SMC to the LMC and to the globular clusters. The BL+WV samples have the slopes, in the K_s -band, of -2.113 ± 0.125 ,

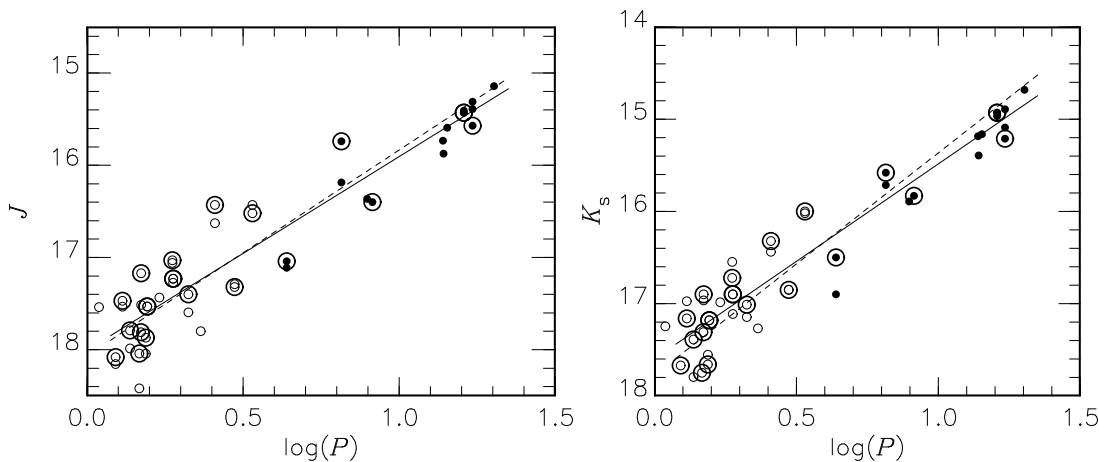


Figure 3. Period-luminosity relations in J and K_s for the combined IRSF and NTT (C10) dataset. BL and WV stars are indicated by open and filled circles and those taken from Ciechanowska et al. (2010) are encircled in addition. The solid lines indicate the least squares solutions, while the dashed lines show the relations used by C10 to derive an SMC modulus.

-2.278 ± 0.047 and -2.408 ± 0.047 , and in $W_1(VI)$ for the SMC and LMC the slopes are -2.304 ± 0.107 and -2.521 ± 0.022 . It should be noted, on the other hand, that the slopes of either the BLs or of the WVs taken by themselves are very uncertain due to the small period range and the relatively small number of stars in each group. The difference in slope between systems may be caused by metallicity and/or age effects although these parameters of the T2Cs are unknown for the Magellanic Clouds. Evidently an SMC distance, and to a lesser extent an LMC distance, based on the cluster data will vary according to the period at which the comparison is made.

4 THE DISTANCE DIFFERENCE BETWEEN THE MAGELLANIC CLOUDS

4.1 Possible effects of Magellanic Cloud structure

The Magellanic Clouds are close enough to us that their three dimensional structure could affect the relative mean distance of different groups of stars. These structures have been studied using several tracers: e.g. classical Cepheids (e.g. Caldwell & Coulson 1986; Groenewegen 2000), red variables (Lah, Kiss & Bedding, 2005) and red-clump giants (Subramanian & Subramanian 2009). These authors discussed the internal structures of the Clouds, especially a large line-of-sight depth and substructures of the SMC. Fig. 4 plots the deviations, $\Delta\mu_0$, from the $\log P$ - $W_1(VI)$ relation against Right Ascension and Declination for both Clouds. We used the PLRs derived for the BLs and WVs separately to estimate their $\Delta\mu_0$ values. These plots are similar to those for classical Cepheids (Fig. A2). In particular the spread is much wider for the SMC than for the LMC due to its large depth. Other major features known from the classical Cepheids are also seen in the T2Cs; e.g. the north-east part of the SMC is closer than the main body. The apparent larger scatter for the BLs compared with the WVs in the SMC may not be significant (see Section 3.1). The zero points of the PLRs correspond to the barycentres of the whole sample, which are indicated by the horizontal lines in Fig. 4 and A2. The distances discussed in the following refer to these barycentres.

Table 3. The SMC-LMC modulus difference ($\Delta\mu_0$) derived from the PLRs of T2Cs and classical Cepheids. No corrections for metallicity effects have been applied.

Type (or $\log P$ range)	from K_s	$\Delta\mu_0$ from $W_1(VI)$	from $W_2(VI)$
Type II Cepheids			
BL	0.19 ± 0.07	0.24 ± 0.07	0.23 ± 0.07
WV	0.40 ± 0.07	0.39 ± 0.05	0.38 ± 0.04
BL+WV	0.38 ± 0.11	0.45 ± 0.08	0.44 ± 0.08
Classical Cepheids			
0.0–0.4	0.530 ± 0.012	0.543 ± 0.009	0.537 ± 0.010
0.4–1.0	0.484 ± 0.008	0.482 ± 0.008	0.476 ± 0.008
1.0–1.7	0.478 ± 0.025	0.486 ± 0.025	0.479 ± 0.024
0.4–1.7	0.495 ± 0.011	0.484 ± 0.010	0.480 ± 0.009

4.2 The distance difference from the PLRs of Cepheids

In view of the results of Section 3.2 we have derived the difference in moduli of the two Clouds independently for the BLs and WVs. This minimizes any effect on the results of the choice of slopes for PLRs. In this section we also compare these results with those for fundamental mode, classical Cepheids, using the results of Appendix A. For both types of Cepheids, the samples were collected from the same datasets: the OGLE-III variability search in the optical and the IRSF survey in the near-IR.

Table 3 compares the $\Delta\mu_0$ values, in K_s and $W(VI)$, from the classical Cepheids and the T2Cs. The $\Delta\mu_0$ are estimated individually for the groups with different period ranges: three groups with the thresholds of 0.4 and 1.0 in $\log P$ for classical Cepheids, and BL ($\log P < 0.6$) and WV ($\log P > 0.6$) for T2Cs. We here consider the K_s -band PLR for the SMC obtained for the combined datasets of C10 and ours, but the results are not affected if only our photometry is used. In the use of the K_s -band PLR, we make a corrections for extinctions of $E_{B-V} = 0.074$ and 0.054 for the LMC and SMC respectively (Caldwell & Coulson 1985) according to the extinction law of Cardelli et al. (1989).

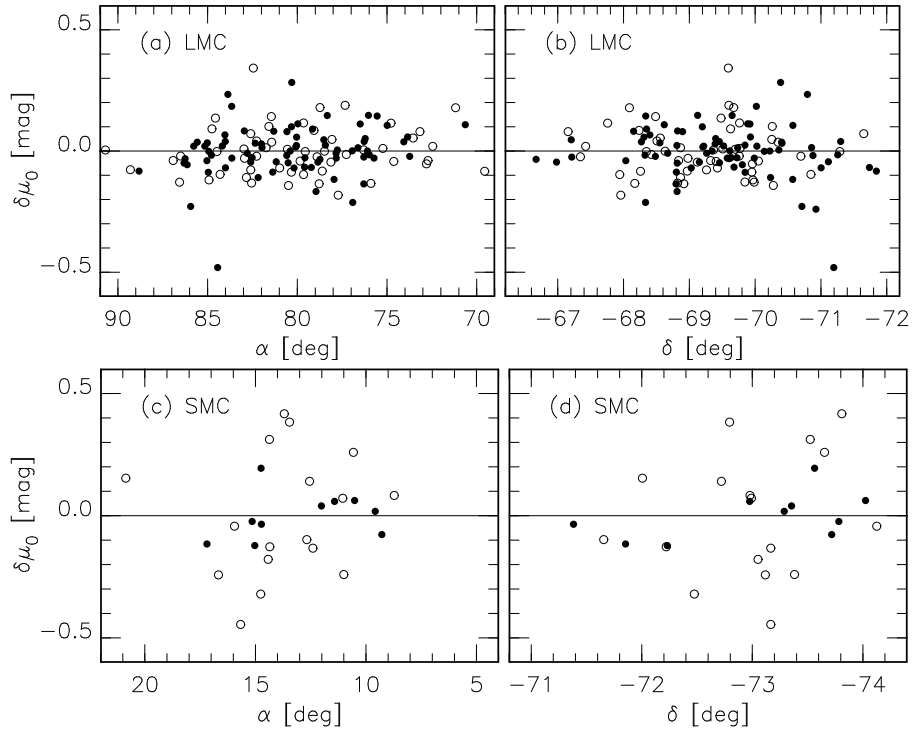


Figure 4. The scatter of the distance moduli of individual T2Cs in the LMC, panels (a) and (b), and in the SMC, (c) and (d) plotted against Right Ascension and Declination. BL and WV stars are indicated by open and filled circles. The horizontal lines indicate the barycentres which are determined by the PLRs. A positive $\delta\mu_0$ means that the object is more distant than the centre.

4.2.1 $\Delta\mu_0$ from classical Cepheids

For the classical Cepheids with $\log P > 0.4$ the results agree well with previous estimates (e.g. Groenewegen 2000). A larger $\Delta\mu_0$ value is indicated at the shorter periods. In the SMC, the PLR slopes at these short periods are different from the longer period ones. This is not the case in the LMC. This suggests that they are less suitable for measuring distance differences at least in the LMC/SMC metallicity range (see also Appendix A).

Metallicity effects on the PLRs of classical Cepheids have been the subject of many publications. On the observational side, two methods are frequently used: (i) comparing Cepheids located in a galaxy at different distances from its centre and thus characterized by different abundances (e.g. Freedman & Madore 1990; Macri et al. 2006; Scowcroft et al. 2009), and (ii) comparing Cepheid-based distances with those obtained with an independent distance indicator, most often the tip of Red Giant Branch (RGB) (e.g. Sakai et al. 2004; Bono et al. 2010). Recently, Bono et al. (2010) investigated the metallicity effects on the PLRs of classical Cepheids from both the observational and theoretical sides and found that these effects were small in $W(VI)$ for a broad range of metallicities. Taking into account estimates in the literature, we consider here a range in the metallicity effect of 0 to $-0.3 \text{ mag dex}^{-1}$, for the classical Cepheids with $\log P > 0.4$. The metallicity difference between the Clouds, $\sim 0.4 \text{ dex}$ (Romaniello et al. 2008), leads to the correction of 0–0.1 mag. We adopt a mean value, i.e. $0.05 \pm 0.05 \text{ mag}$, which leads to a metallicity corrected value of $\Delta\mu_0^{\text{cor}} = 0.43 \pm 0.05 \text{ mag}$. The error is dominated by the uncertainty of the metallicity correction.

4.2.2 $\Delta\mu_0$ from type II Cepheids

No theoretical predications seem to have been made for metallicity effects for T2Cs. However, the results for T2Cs in globular clusters (M06), which are heavily weighted to WV stars, suggests that at K_s any such effects are small. The present results support this conclusion since the $\Delta\mu_0$ values for the WV stars in Table 3 are in satisfactory agreement with the metallicity corrected value for the longer period classical Cepheids.

On the other hand, the $\Delta\mu_0$ value from the BL stars is smaller than for the WVs or classical Cepheids. This is a result at the 2σ level and is present both in K_s and VI . This points to a difference in mean properties of BLs in the LMC and SMC. Mean metallicity or age differences are the most likely candidates.

4.3 Comparison with other methods

Various other estimates of the difference in the distance moduli of the Clouds, $\Delta\mu_0$, are listed in Table 4. This table also shows the results for WV stars, and the longer period classical Cepheids.

Szewczyk et al. (2008, 2009) used near-IR PLRs of RR Lyraes to derive the distance moduli of the Clouds. They adopted mean metallicities for the LMC and SMC RR Lyraes of -1.48 and -1.7 dex . This leads to changes in $\Delta\mu_0$ of 0.02–0.05 mag depending on which metallicity dependent calibration of the PLR is adopted. These corrections bring the difference into better agreement with the WVs and classical Cepheids. Interestingly, the metallicity correction for RR Lyraes has the same sign as that suggested for BLs above.

Hilditch, Howarth & Harries (2005) obtained an SMC distance modulus of $18.91 \pm 0.1 \text{ mag}$ from eclipsing binaries, while a larger value, $19.11 \pm 0.03 \text{ mag}$, was obtained by North et al. (2010).

Table 4. The SMC-LMC modulus difference, $\Delta\mu_0$, derived in various ways. The values corrected for metallicity and/or other population effects, $\Delta\mu_0^{\text{cor}}$, are also listed. Their errors include the uncertainty of this correction. References are indicated in the last column.

Method	$\Delta\mu_0$	$\Delta\mu_0^{\text{cor}}$	Notes	Ref.
Type II Cepheids (WV)	0.40 ± 0.07	—	(1)	This work
	0.39 ± 0.05	—	(2)	This work
Classical Cepheids	0.48 ± 0.01	0.43 ± 0.05	(1,3,4)	This work
	0.48 ± 0.01	0.43 ± 0.05	(2,3,4)	This work
	0.48 ± 0.04	0.43 ± 0.06	(1,3)	Groenewegen (2000)
	0.51 ± 0.02	0.46 ± 0.05	(2,3)	Groenewegen (2000)
	0.41 ± 0.20	0.39 ± 0.20	(1)	Bono et al. (2010)
	0.45 ± 0.12	0.44 ± 0.12	(2)	Bono et al. (2010)
RR Lyrae variables	0.327 ± 0.002	0.363 ± 0.04	(1,5)	Szewczyk et al. (2009)
Red clump giants	0.47 ± 0.03	0.43	(1,6)	Pietrzyński et al. (2003)
	0.38 ± 0.02	0.45 ± 0.10	(2)	Pietrzyński et al. (2003)
Tip of RGB	—	0.40 ± 0.12	(2,7)	Sakai et al. (2004)
Pulsating M giants	0.41 ± 0.02	—	(1,8)	Tabur et al. (2010)
Eclipsing binaries	—	0.5 ± 0.15	(9)	—

Notes: (1) Based on near-IR photometry, K_s or K . (2) Based on optical photometry, I or $W(VI)$. (3) Our adopted metallicity correction, 0–0.1 mag, was used to derive $\Delta\mu_0^{\text{cor}}$. (4) Only those with $0.4 < \log P < 1.0$ were used. (5) Taking the means of the values based on different calibrations discussed in Szewczyk et al. (2009). (6) The population correction suggested by Salaris & Girardi (2002) was used. (7) A metallicity correction was derived using the colour of the RGB. (8) Tabur et al. (2010) concluded that the metallicity effect is negligible. (9) This value is a rough estimate (see text).

The difference in these values may come partly from the internal structure of the SMC, but other factors seem to be involved. One of these is the use of different surface brightness-colour relations. These tend to be especially uncertain for the early type binaries which have generally been used. The method is also sensitive to reddening estimates. The available distance estimates for the LMC from early type binaries show a rather large scatter (see e.g. Nelson et al. 2000). Pietrzyński et al. (2009) derived an LMC distance modulus of 18.50 ± 0.06 based on a binary system composed of two late-type giants. In Table 4, $\Delta\mu_0 \approx 0.5 \pm 0.15$ mag is adopted.

For red clump stars, Pietrzyński, Gieren & Udalski (2003) obtained $\Delta\mu_0 = 0.47 \pm 0.03$ mag from K magnitudes. A population correction by Salaris & Girardi (2002) leads to 0.43 mag. Tabur et al. (2010) compared the PLR sequences of pulsating M-type giants, i.e. semi-regulars and Miras, in the Magellanic Clouds and those in the solar neighbourhood, finding $\Delta\mu_0 = 0.41 \pm 0.02$ mag. They concluded that the metallicity effect for their PLRs is negligible.

In summary, the mean uncorrected $\Delta\mu_0$ for the WVs is 0.39 ± 0.05 mag. This agrees well with the other results in Table 4. These, corrected for metallicity and age effects where necessary, range from 0.36 to 0.46 mag (while eclipsing variables giving ~ 0.5 mag). Thus any effect due to population differences on the WVs appear to be small. On the other hand, the smaller $\Delta\mu_0$ for the BLs, together with the result shown in Fig. 3, suggests that the population difference between the two Clouds is affecting the mean luminosities of these stars.

5 THE PERIODS AND COLOURS OF TYPE II CEPHEIDS IN DIFFERENT SYSTEMS

5.1 Period distribution of type II Cepheids

Fig. 5 compares the period distributions of the T2Cs in the Magellanic Clouds and in globular clusters. The pW stars are not included in this comparison. The sample for globular clusters has

been slightly changed from that in M09 to include the T2Cs in NGC 6388 and 6441 (table 7 in Pritzl et al. 2003).

A separation between WV and RV stars is evident for the LMC and SMC samples, while the distribution of the cluster sample suggests that the stars in the RV period range are just the tail of the WV star distribution. This together with the fact that cluster variables in the RV period range lie on an extension of the cluster T2C PLR indicates a fundamental difference from those in the Clouds which lie about PLRs fitted to shorter period T2Cs. There is a suggestion that the relative frequency of variables with $\log P \sim 0.8$ is greater in the LMC than the clusters.

There is a difference in the relative frequencies of WV and BL stars between the LMC and the SMC. The ratio of the two types, $N_{\text{WV}}/N_{\text{BL}}$, is 1.25 ± 0.2 for the LMC and 0.6 ± 0.2 for the SMC, where the Poisson noise is considered as the uncertainty. Although the LMC ratio changes if we exclude the conspicuous group of the LMC WV stars with $\log P \sim 0.8$, it would still be larger than the ratio for the SMC. To test for a metallicity effect in this ratio, the globular cluster sample was divided into three groups: 11 objects with $[\text{Fe}/\text{H}] < -1.9$, 53 with $-1.9 < [\text{Fe}/\text{H}] < -1.0$ and 13 with $[\text{Fe}/\text{H}] > -1$ dex. Fig. 6 plots the periods of the globular T2Cs against their metallicities (taken from Harris 1996). We do not include in the discussion the objects in ω Cen, indicated by the cross symbols in Fig. 6, because this cluster has a significant spread in $[\text{Fe}/\text{H}]$. Adopting $P = 4, 20$ d as the dividing lines of the T2C types, $N_{\text{WV}}/N_{\text{BL}}$ are 0.1 ± 0.1 , 1.9 ± 0.6 and 1.0 ± 0.6 for the three groups. The sample in the most metal-rich range is dominated by NGC 6388 and 6441, the two metal-rich clusters with a peculiar population of RR Lyrae stars (Pritzl et al. 2003). Comparing the WV/BL ratios between the other two metallicity ranges suggests that a metal-poor stellar system has a lower WV/BL ratio. This is qualitatively consistent with above results if the SMC T2Cs are lower in metallicity than the LMC ones. Further discussion will be possible when metallicities have been determined for T2Cs in the Magellanic Clouds.

It is interesting that the ratio of long-period to short-period stars is also greater in the LMC than in the SMC for the classi-

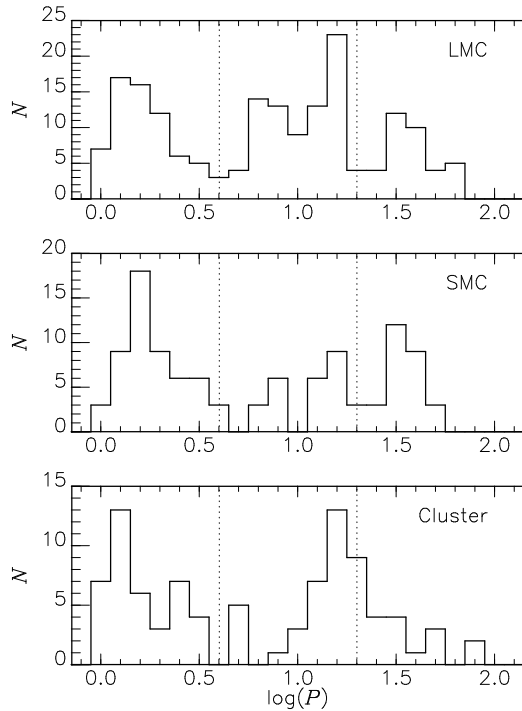


Figure 5. Histograms of periods for the T2Cs in the LMC (top), SMC (middle) and globular clusters (bottom). The pW stars are not included. Vertical lines show the thresholds, 4 and 20 d, used to divide BL, WV and RV variables.

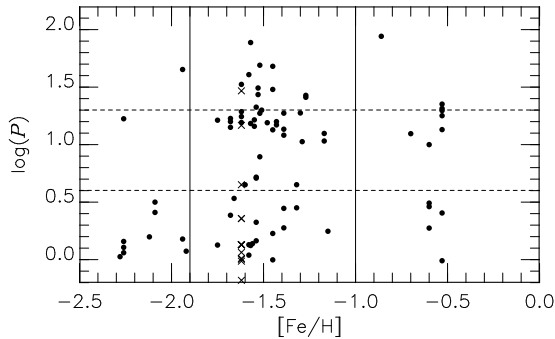


Figure 6. Periods and metallicities of the T2Cs in globular clusters. The cross symbols indicate those in ω Cen plotted at its mean metallicity. The horizontal lines show the divisions between the BL, WV and RV stars, and the vertical lines the adopted divisions by metallicity (see text).

cal Cepheids (Soszyński et al. 2010a; also see Appendix A). This has generally been attributed to a metallicity effect (Becker, Iben & Tuggle, 1977). Although not included in Fig. 5, the SMC pW stars have longer periods than their counterparts in the LMC as pointed out in S10 and as can be seen from Fig. A1. The reason for this is not clear. No counterpart to pW stars have been identified in globular clusters.

5.2 Colours of type II Cepheids

Fig. 7 shows colour-magnitude and colour-colour diagrams for BL, WV, pW and RV variables in the SMC. T2Cs in globular clusters are plotted by grey star symbols in the colour-colour diagrams for

comparison. In panel (d), the triangles indicate Galactic RV stars from Lloyd Evans (1985). Their magnitudes were converted from the SAAO system into that of the IRSF using transformations in Carpenter (2001) and Kato et al. (2007). For the cluster variables, the dereddened colours have been adjusted for the mean SMC reddening ($E_{B-V} = 0.054$ mag, Caldwell & Coulson 1985). The colours of the Galactic RV stars have not been corrected for their reddenings. The curves in the two-colour plots indicate the location of normal giants (G0III–K5III) taken from Bessell & Brett (1988) whose colours are also transformed into the IRSF system after adding the SMC reddening. The distribution of the SMC objects in these plots is similar to that of the LMC objects (fig. 3 in M09).

Infrared colour/ $\log P$ relations are plotted in Fig. 8. No correction for interstellar reddening was applied to the SMC objects. The dereddened magnitudes of the globular cluster objects have been reddened by an amount corresponding to the SMC reddening as in Fig. 7, so that the two samples are directly comparable. The WV stars in globular clusters, $1.0 \leq \log P \leq 1.3$, have a trend for $(J - H)$ and $(J - K_s)$ to become bluer with increasing period, which is not clear for the SMC WVs. Two pW stars in the SMC, #1 and #11, are separated from the trend of globular WV stars. The lower photometric accuracies for BL stars prevent us from any comparison with the clusters.

RV stars show a wider colour distribution and appear to be heterogeneous in nature (see section 5.2 in M09). An SMC RV star, #18, is distinctly red in $J - K_s$ and $H - K_s$ but not in $J - H$. A few RV stars are similar to the globular objects in $H - K_s$ but bluer in $J - H$ at a given period. These features of the SMC T2Cs are similar to those in the LMC (M09). On the other hand, the two brightest stars, RV stars #7 and #29, are not exceptionally red in any near IR colour. This is different from the situation in the LMC where the three brightest RV stars have an excess in K_s (M09) as does the SMC RV star #18. In the $\log P - K_s$ plot (Fig. A1) #7 and #29 are almost as bright as classical Cepheids with similar periods (see Fig. A1). S10 notes that these two stars are in binary, eclipsing or ellipsoidal, systems.

6 CONCLUSIONS

In this paper PLRs are derived for T2Cs in the SMC. Evidence is presented that T2C PLR slopes differ in three different systems (globular clusters, LMC, SMC) when BL and WV stars are used in combined solutions. Treating the BL and WV stars separately, it was found that the difference in distance moduli between the SMC and LMC derived from WVs alone agrees closely with that obtained from other distance indicators. This implies that the absolute magnitudes of the WVs are, within the uncertainties, free of metallicity effects, which is in agreement with the results derived from globular clusters. On the other hand the SMC-LMC difference is smaller for the BLs and suggests that their absolute magnitudes are not immune from population effects. The relative frequencies of WV to BL stars also varies from system to system.

ACKNOWLEDGMENTS

This work is based on the result of the OGLE project. The OGLE has received funding from the European Research Council under the European Community's Seventh Framework Programme (FP7/2007-2013)/ERC grant agreement no. 246678. We thank the referee (G. Bono) for his useful comments. NM acknowledges

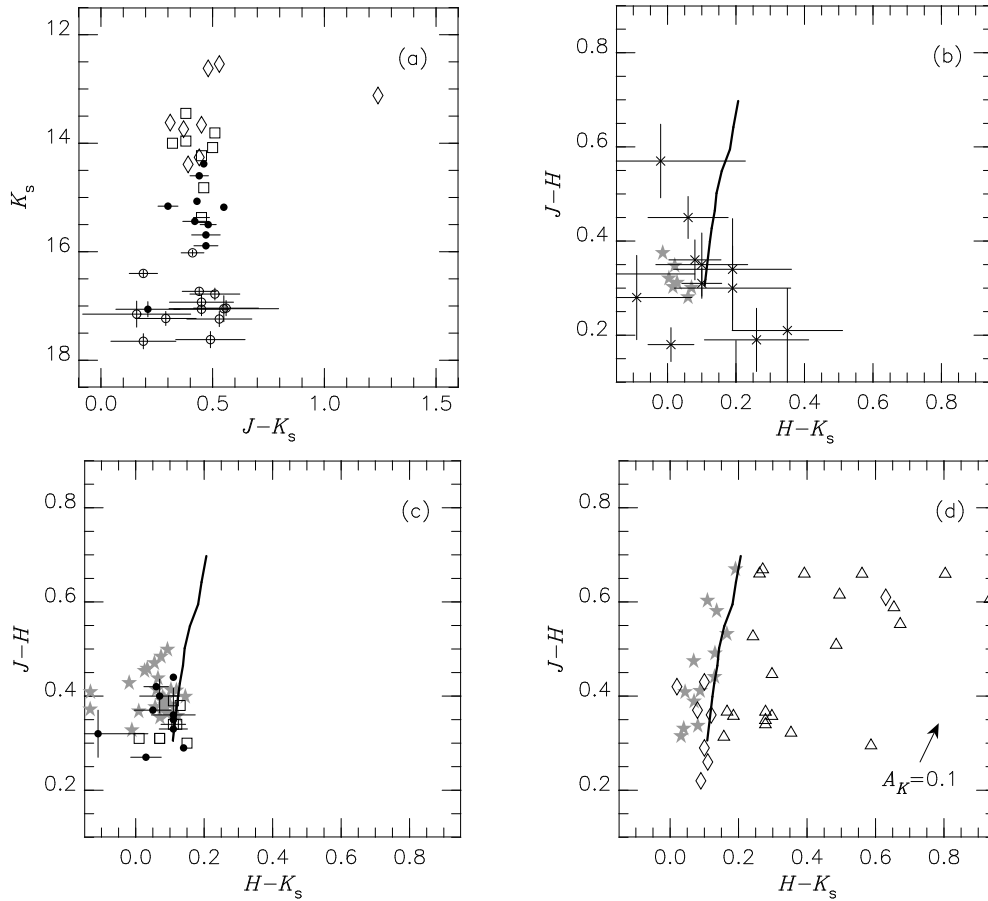


Figure 7. A colour-magnitude diagram and colour-colour diagrams for T2Cs. Panel (a) includes all types SMC T2Cs, while panels (b), (c) and (d) are for BL, WV/pW and RV stars. Symbols for the SMC T2Cs are the same as in Fig. 2. Grey star symbols indicate the T2Cs in globular clusters (M06). In panel (d), the triangles are for Galactic RV stars from Lloyd Evans (1985). Error bars are drawn for the SMC T2Cs only if an uncertainty exceeds the size of the symbol. The thick curve in the colour-colour diagrams is the locus of local giants from Bessell & Brett (1988).

the support by the Grant-in-Aid for Research Activity Start-up (No. 22840008) from the Japan Society for the Promotion of Science (JSPS). The work of MWF is supported by South African National Research Foundation.

REFERENCES

Baade W., 1952, *Trans. IAU*, 8, 682
 Bauer F et al. (EROS collaboration), 1999, *A&A*, 348, 175
 Becker S. A., Iben I., Tuggle R. S., 1977, *ApJ*, 218, 633
 Bessell M. S., Brett J. M., 1988, *PASP*, 100, 1134
 Bono G., Marconi M., 1999, *IAUS*, 190, 527
 Bono G., Caputo F., Marconi M., Musella I., 2010, *ApJ*, 715, 277
 Caldwell J. A. R., Coulson I. M., 1985, *MNRAS*, 212, 879
 Caldwell J. A. R., Coulson I. M., 1986, *MNRAS*, 218, 223
 Cardelli J. A., Clayton G. C., Mathis J. S., 1989, *ApJ*, 345, 245
 Carpenter J. M., 2001, *AJ*, 121, 2851
 Ciechanowska A., Pietrzyński G., Szewczyk O., Gieren W., Soszyński I., 2010, *Acta Astron.*, 60, 233
 Dolphin A. E. et al., 2003, *AJ*, 125, 1261
 Feast M. W., Laney C. D., Kinman T. D., van Leeuwen F., Whitelock P. A., 2008, *MNRAS*, 386, 2115
 Fernie J. D., 1969, *PASP*, 81, 707
 Freedman W. L., Madore B. F., 1990, *ApJ*, 365, 186

Gingold R. A., 1976, *ApJ*, 204, 116
 Gingold R. A., 1985, *Mem. Soc. Astron. Ital.*, 56, 169
 Groenewegen M. A. T., 2000, *A&A*, 363, 901
 Harris W. E., 1996, *AJ*, 112, 1487
 Hilditch R. W., Howarth I. D., Harries T. J., 2005, *MNRAS*, 357, 304
 Kato D. et al., 2007, *PASJ*, 59, 615
 Lah P., Kiss L. L., Bedding T. R., 2005, *MNRAS*, 359, L42
 Lloyd Evans T., 1985, *MNRAS*, 217, 493
 Macri L. M., Stanek K. Z., Bersier D., Greenhill L. J., Reid M. J., 2006, *ApJ*, 652, 1133
 Marengo M., Evans N. R., Barmby P., Bono G., Welch D. L., Romaniello M., 2010, *ApJ*, 709, 120
 Matsunaga N. et al., 2006, *MNRAS*, 370, 1979 (M06)
 Matsunaga N., Feast M. W., Menzies J. W., 2009, *MNRAS*, 397, 933 (M09)
 Nelson C. A., Cook K. H., Popowski P., Alves D. R., 2000, *AJ*, 119, 1205
 Ngeow C.-C., Kanbur S. M., 2010, *ApJ*, 720, 626
 Ngeow C.-C., Kanbur S. M., Neilson H. R., Nanthakumar A., Buonaccorsi J., 2009, *ApJ*, 693, 691
 North P. L., Gauderon R., Barblan F., Royer F., 2010, *A&A*, 520, 74
 Pietrinferni A., Cassisi S., Salaris M., Castelli F., 2006, *ApJ*, 642, 797

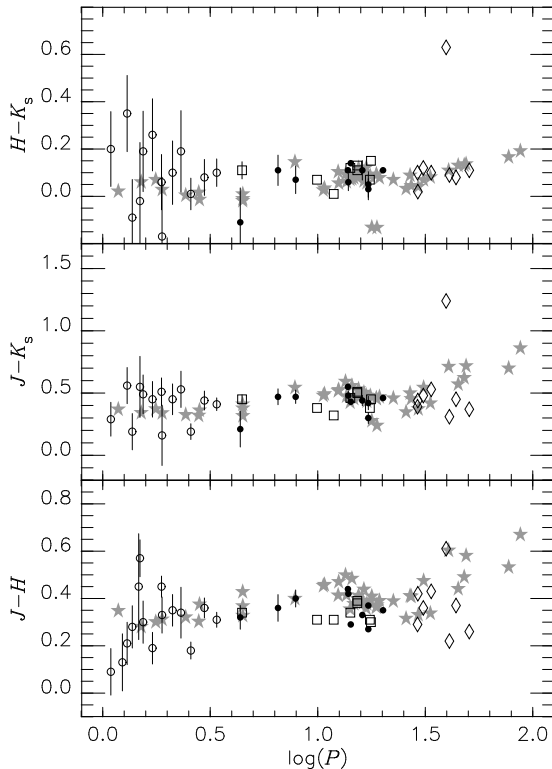


Figure 8. Period-colour relations for T2Cs. Symbols are the same as in Fig. 7. Error bars are indicated for the SMC T2Cs only if the uncertainties exceed 0.03 mag.

- Pietrzyński G., Gieren W., Udalski A., 2003, *AJ*, 125, 2494
 Pietrzyński G. et al., 2009, *ApJ*, 697, 862
 Pritzl B. J., Smith H. A., Stetson P. B., Catelan M., Sweigart A. V., Layden A. C., Rich R. M., 2003, *AJ*, 126, 1381
 Romaniello M. et al., 2008, *A&A*, 488, 731
 Sakai S., Ferrarese L., Kennicutt R. C., Saha A., 2004, *ApJ*, 608, 42
 Salaris M., Girardi L., 2002, *MNRAS*, 337, 332
 Sandage A., Tammann G. A., 2006, *ARA&A*, 44, 93
 Sandage A., Tammann G. A., Reindl B., 2009, *A&A*, 493, 471
 Scowcroft V., Bersier D., Mould J. R., Wood, P. R., 2009, *MNRAS*, 396, 1287
 Skrutskie M. F. et al., 2006, *AJ*, 131, 1163
 Soszyński I. et al., 2008a, *Acta Astron.*, 58, 163
 Soszyński I. et al., 2008b, *Acta Astron.*, 58, 293
 Soszyński I. et al., 2010a, *Acta Astron.*, 60, 17
 Soszyński I. et al., 2010b, *Acta Astron.*, 60, 91 (S10)
 Subramanian S., Subramaniam A., 2009, *A&A*, 496, 399
 Szewczyk O. et al., 2008, *AJ*, 136, 272
 Szewczyk O., Pietrzyński G., Gieren W., Ciechanowska A., Bresolin F., Kudritzki R. P., 2009, *AJ*, 138, 1661
 Tabur V., Bedding T. R., Kiss L. L., Giles T., Derakas A., Moon T. T., 2010, *MNRAS*, 409, 777
 Thackeray A. D., Wesselink A. J., 1953, *Natur*, 171, 693
 Wallerstein G., 2002, *PASP*, 114, 689

APPENDIX A: THE PLRS OF CLASSICAL CEPHEIDS

For comparison with the T2Cs, PLRs have been derived for the classical Cepheids in both Clouds found in the OGLE III survey (Soszyński et al. 2008a; Soszyński et al. 2010a). Choosing fundamental mode pulsators only there are 1849 stars in the LMC and 2626 in the SMC. Of these, there are matches within $0.5''$, for 1797 and 2436 stars in the IRSF catalogue (Table A1). Among these, 140 and 187 stars were detected in the IRSF survey twice because they are located in overlapping fields of the IRSF survey. These duplicates show that the phase-correction procedure which gives satisfactory results for the T2Cs does not work well for the classical Cepheids. This is probably because of systematically different light curves in I and in JHK_s for the latter. We thus use the single-epoch IRSF magnitudes to discuss the near-IR PLRs. This has a negligible effect on the final results because of the large number of stars involved.

Fig. A1 shows the K_s -band PLRs of the classical Cepheids in the both Clouds. Those for the T2Cs are also plotted. Classical Cepheids are brighter than T2Cs by 1.0–2.5 mag depending on the periods. The pW/RV stars are located between the PLRs of two types of Cepheids.

The classical Cepheids in each galaxy were divided into three groups according to their periods using divisions at 0.4 and 1.0 in $\log P$. For each group and period range, a least-square fit was obtained with a 3σ clipping applied. (Table A2). Note that no correction of interstellar extinction has been applied (they are of course unnecessary in $W(VI)$).

A break in the slope of the PLR at $\log P \sim 0.4$, was first found by Bauer et al. (1999) and confirmed by later work (Soszyński et al. 2010a; and references therein). A break at around $\log P = 1$ has been also claimed especially at optical wavelengths (see e.g. Sandage, Tammann & Reindl, 2009). The latter break is less certain than the former and is expected to be less significant, and possibly absent, in the near-IR (see table 2 in Bono et al. 2010). It is also not present in $W(VI)$ (Bono & Marconi 1999).

The PLRs in the shortest period range, $0.0 < \log P < 0.4$, are steeper than those at longer periods in the SMC, but not in the LMC. The slope change seems to be a characteristic of Cepheids in a low-metal environment like the SMC and dwarf galaxies (Dolphin et al. 2003). This break has been also confirmed in the *Spitzer* photometry at the $3.6 \mu\text{m}$ and $4.5 \mu\text{m}$ bands (Ngeow & Kanbur 2010). On the other hand, the slopes for the PLRs at $0.4 < \log P < 1.0$ and $\log P > 1.0$ are nearly the same and the break at $\log P \sim 1$ is not evident in these data. This is also consistent with previous studies involving the infrared PLRs (Ngeow et al. 2009; Ngeow & Kanbur 2010; Marengo et al. 2010).

The residuals of individual classical Cepheids from the PLRs in $W_1(VI)$ for each group are plotted in Fig. A2. As in Fig. 4, the distribution for the SMC objects show a larger scatter than that in the LMC and a clear spatial structure. One can also notice a small tilt of the distribution in the LMC, which is barely seen for the T2Cs (Fig. 4). The eastern part of the LMC disk is slightly closer to us than the western part in agreement with previous work (Caldwell & Coulson 1986; Groenewegen 2000).

Table A1. The catalogue of OGLE-III classical Cepheids, pulsating in the fundamental mode, with IRSF counterparts. The periods and corresponding IRSF measurements are listed as in Table 1. Shifts for the phase corrections (δ_ϕ) obtained from the *I*-band light curves are also listed, but not used in our plots and fits. This is the first 10 lines of the full catalogue which will be available in the online version of the article (see Supporting Information). Note that both the LMC and SMC objects are included in a single catalogue, but each OGLE-ID indicates one of the Clouds.

OGLE-ID	$\log P$	IRSF-Field		IRSF counterpart							δ_ϕ
		IRSF-Field	MJD(obs)	Phase	<i>J</i>	<i>E_J</i>	<i>H</i>	<i>E_H</i>	<i>K_s</i>	<i>E_{K_s}</i>	
OGLE-LMC-CEP-0028	0.10139	LMC0443-6940F	53036.771	0.844	16.34	0.03	16.07	0.03	15.95	0.08	-0.169
OGLE-LMC-CEP-0033	0.85617	LMC0444-6920C	53036.877	0.068	13.72	0.02	13.45	0.01	13.38	0.02	0.177
OGLE-LMC-CEP-0034	1.05133	LMC0442-7040E	52693.855	0.645	13.23	0.02	12.84	0.01	12.71	0.02	-0.165
OGLE-LMC-CEP-0040	0.71308	LMC0443-6940C	53034.803	0.132	13.99	0.01	13.74	0.01	13.70	0.02	0.191
OGLE-LMC-CEP-0042	0.41112	LMC0442-7020H	52692.889	0.978	14.99	0.01	14.87	0.02	14.80	0.02	0.262
OGLE-LMC-CEP-0042	0.41112	LMC0443-7000B	53039.905	0.635	15.26	0.01	14.96	0.02	14.90	0.03	-0.174
OGLE-LMC-CEP-0046	0.94663	LMC0444-6920H	53498.715	0.522	13.47	0.02	13.08	0.02	12.99	0.01	-0.117
OGLE-LMC-CEP-0048	0.74418	LMC0443-6940E	53034.855	0.166	13.85	0.01	13.57	0.01	13.52	0.02	0.145
OGLE-LMC-CEP-0049	0.58536	LMC0442-7040D	52692.971	0.257	14.67	0.02	14.33	0.01	14.24	0.03	0.028
OGLE-LMC-CEP-0050	0.89463	LMC0443-6940H	53037.841	0.805	13.81	0.02	13.42	0.02	13.34	0.03	-0.164

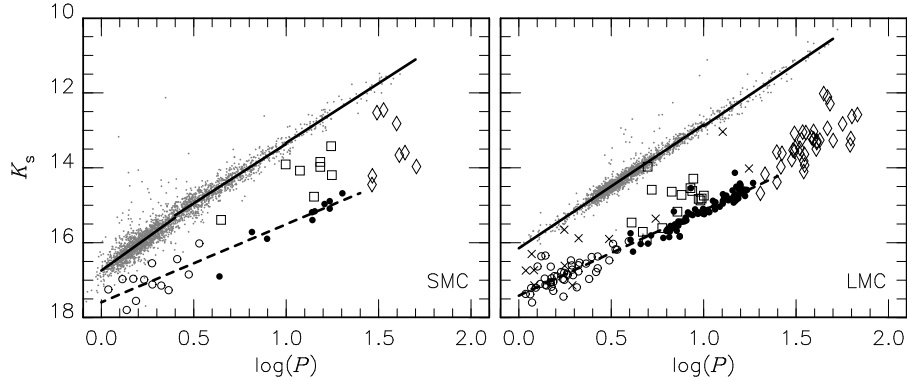


Figure A1. The PLRs at K_s for classical Cepheids in the SMC(left) and LMC (right) (grey dots and filled lines, see Appendix A). Also shown for comparison are the relations for the T2Cs, indicated by dashed lines. Symbols for the T2Cs are the same as in Fig. 2 except the crosses in the LMC sample which indicate stars not used in the least squares fits (see M09). RVs and pWs are shown as open circles and squares.

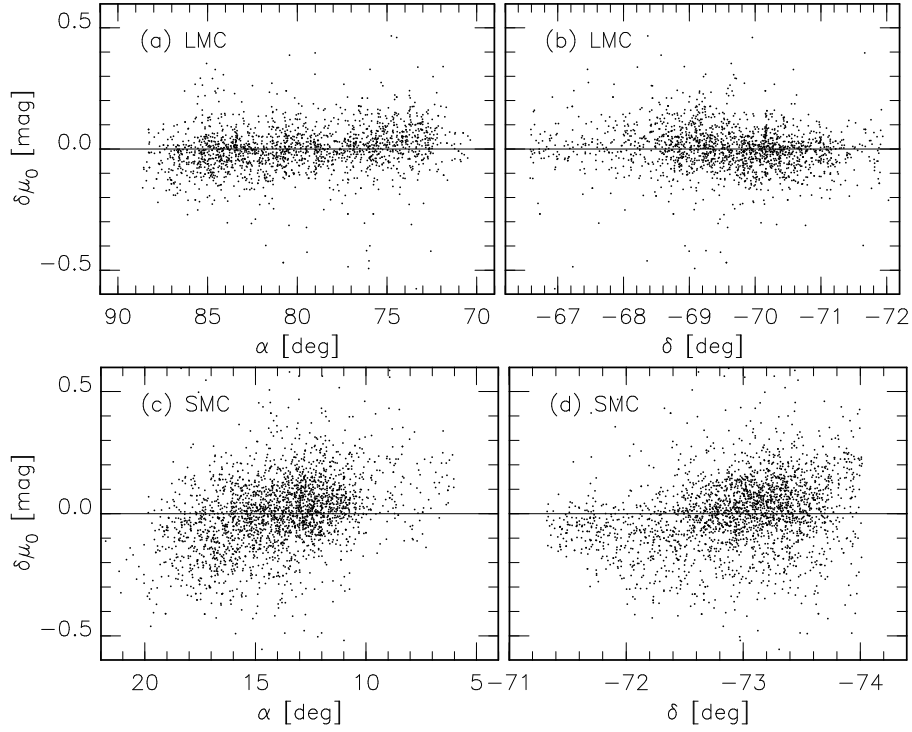


Figure A2. The scatter in the distance moduli of individual classical Cepheids in the LMC, panels (a) and (b), and SMC, (c) and (d). Refer to the caption of Fig. 4.

Table A2. Period-luminosity relations for classical Cepheids. Refer to the caption of Table 2.

Band	Group	Period range	Slope	Zero (@ $\log P_0$)	σ	N
<i>J</i>	LMC	$0.0 < \log P < 0.4$	-3.139 ± 0.124	15.522 ± 0.012 (@ 0.3)	0.16	164
<i>J</i>	LMC	$0.4 < \log P < 1.0$	-3.138 ± 0.028	14.254 ± 0.005 (@ 0.7)	0.16	1585
<i>J</i>	LMC	$1.0 < \log P < 1.7$	-3.053 ± 0.165	12.719 ± 0.020 (@ 1.2)	0.21	119
<i>H</i>	LMC	$0.0 < \log P < 0.4$	-3.235 ± 0.099	15.231 ± 0.010 (@ 0.3)	0.13	164
<i>H</i>	LMC	$0.4 < \log P < 1.0$	-3.248 ± 0.022	13.926 ± 0.004 (@ 0.7)	0.12	1579
<i>H</i>	LMC	$1.0 < \log P < 1.7$	-3.143 ± 0.139	12.336 ± 0.017 (@ 1.2)	0.18	120
<i>K_s</i>	LMC	$0.0 < \log P < 0.4$	-3.289 ± 0.099	15.160 ± 0.010 (@ 0.3)	0.13	164
<i>K_s</i>	LMC	$0.4 < \log P < 1.0$	-3.284 ± 0.020	13.838 ± 0.004 (@ 0.7)	0.11	1584
<i>K_s</i>	LMC	$1.0 < \log P < 1.7$	-3.197 ± 0.135	12.231 ± 0.017 (@ 1.2)	0.17	118
<i>W₁(VI)</i>	LMC	$0.0 < \log P < 0.4$	-3.325 ± 0.078	14.906 ± 0.008 (@ 0.3)	0.10	160
<i>W₁(VI)</i>	LMC	$0.4 < \log P < 1.0$	-3.316 ± 0.015	13.573 ± 0.003 (@ 0.7)	0.08	1578
<i>W₁(VI)</i>	LMC	$1.0 < \log P < 1.7$	-3.189 ± 0.163	11.916 ± 0.020 (@ 1.2)	0.20	121
<i>W₂(VI)</i>	LMC	$0.0 < \log P < 0.4$	-3.300 ± 0.080	14.978 ± 0.008 (@ 0.3)	0.10	160
<i>W₂(VI)</i>	LMC	$0.4 < \log P < 1.0$	-3.294 ± 0.015	13.654 ± 0.003 (@ 0.7)	0.09	1579
<i>W₂(VI)</i>	LMC	$1.0 < \log P < 1.7$	-3.159 ± 0.160	12.010 ± 0.019 (@ 1.2)	0.20	121
<i>J</i>	SMC	$0.0 < \log P < 0.4$	-3.381 ± 0.061	16.035 ± 0.008 (@ 0.3)	0.23	1590
<i>J</i>	SMC	$0.4 < \log P < 1.0$	-2.992 ± 0.049	14.720 ± 0.009 (@ 0.7)	0.22	862
<i>J</i>	SMC	$1.0 < \log P < 1.7$	-3.020 ± 0.128	13.171 ± 0.021 (@ 1.2)	0.22	107
<i>H</i>	SMC	$0.0 < \log P < 0.4$	-3.519 ± 0.054	15.744 ± 0.007 (@ 0.3)	0.20	1584
<i>H</i>	SMC	$0.4 < \log P < 1.0$	-3.134 ± 0.042	14.392 ± 0.007 (@ 0.7)	0.19	854
<i>H</i>	SMC	$1.0 < \log P < 1.7$	-3.110 ± 0.114	12.792 ± 0.019 (@ 1.2)	0.19	107
<i>K_s</i>	SMC	$0.0 < \log P < 0.4$	-3.546 ± 0.055	15.683 ± 0.007 (@ 0.3)	0.20	1582
<i>K_s</i>	SMC	$0.4 < \log P < 1.0$	-3.176 ± 0.041	14.315 ± 0.007 (@ 0.7)	0.18	854
<i>K_s</i>	SMC	$1.0 < \log P < 1.7$	-3.197 ± 0.111	12.702 ± 0.018 (@ 1.2)	0.19	108
<i>W₁(VI)</i>	SMC	$0.0 < \log P < 0.4$	-3.543 ± 0.043	15.449 ± 0.005 (@ 0.3)	0.16	1596
<i>W₁(VI)</i>	SMC	$0.4 < \log P < 1.0$	-3.318 ± 0.035	14.055 ± 0.006 (@ 0.7)	0.15	859
<i>W₁(VI)</i>	SMC	$1.0 < \log P < 1.7$	-3.283 ± 0.093	12.402 ± 0.015 (@ 1.2)	0.16	108
<i>W₂(VI)</i>	SMC	$0.0 < \log P < 0.4$	-3.521 ± 0.043	15.515 ± 0.006 (@ 0.3)	0.16	1596
<i>W₂(VI)</i>	SMC	$0.4 < \log P < 1.0$	-3.286 ± 0.035	14.130 ± 0.006 (@ 0.7)	0.16	859
<i>W₂(VI)</i>	SMC	$1.0 < \log P < 1.7$	-3.250 ± 0.093	12.489 ± 0.015 (@ 1.2)	0.16	108